

# Wavelet analysis of stellar differential rotation

## I. The Sun

A. Hempelmann<sup>1</sup> and R.A. Donahue<sup>2,3</sup>

<sup>1</sup> Astrophysikalisches Institut Potsdam, An der Sternwarte 16, D-14482 Potsdam, Germany

<sup>2</sup> Mount Wilson Institute, 740 Holladay Road, Pasadena, CA 91106, USA

<sup>3</sup> Harvard-Smithsonian Center for Astrophysics, 60 Garden Street, MS 15, Cambridge, MA 02138, USA\*

Received 6 September 1996 / Accepted 19 December 1996

**Abstract.** A key mystery in stellar magnetohydrodynamics is knowledge of stellar differential rotation. At present, the only practical method for detecting the presence of surface differential rotation for slowly-rotating stars is through the indirect measurement of the stellar butterfly diagram: i.e., the change of rotation period determined from light modulation caused by the change in mean latitude of stellar surface inhomogeneities, correlated with the phase of the stellar activity cycle. However, finding the correct period is hampered by stellar active region evolution which introduces variability in the amplitude and phase of the modulation. We demonstrate that time-frequency analysis using the wavelet transform is possibly a suitable method for monitoring the stellar butterfly diagram. Wavelet analysis of disk-integrated solar Ca II K line core emission measures shows nearly the correct pattern of the solar surface differential rotation when viewed as a star. This technique can therefore be applied to long-term measurements of stellar activity.

**Key words:** Sun: rotation – stars: late-type – stars: rotation – methods: data analysis

---

### 1. Introduction

The observation of magnetically-induced activity of late-type stars is surely among the most important discoveries of modern astrophysics. Empirical studies which relate the characteristics of stellar activity (photospheric spots, chromospheric plages, and a hot X-ray emitting corona) with basic stellar parameters such as mass, age, and rotation are a natural way to test dynamo theories. Many studies have demonstrated the fundamental importance of stellar rotation for generating the mean activity level whereas the relation between turbulence and stellar activity has not yet been well determined observationally.

---

Send offprint requests to: Alexander Hempelmann  
(ahempelmann@aip.de)

\* Present Address

Stellar rotation and turbulent motions in the stellar interior produce not only a magnetic field, but also lead to differential rotation. The observed  $(r, \theta)$  pattern of the solar rotation (Libbrecht 1988; see also the review by Kennedy (1996) concerning the GONG experiment) is nearly explained by theory (Küker et al. 1993, Rüdiger & Kitchatinov 1994, Kitchatinov & Rüdiger 1995). However, any successful model must also predict the differential rotation of stars other than the Sun.

The observation of surface differential rotation (SDR) of stars is possible via three methods: i) stellar seismology; ii) analysis of the rotational broadening of spectral lines; and iii) observation of stellar ‘butterfly diagrams’. The two latter methods are restricted to delivering only the  $\theta$  dependence of rotation on the stellar surface. Slowly rotating stars like the Sun (2 km/s at the equator) produce a rotational line-broadening which is smaller than the broadening caused by turbulent motions in the stellar photosphere (the radial-tangential macroturbulence ( $\zeta_{RT}$ ); values of  $\zeta_{RT}$  are given by Gray 1988). Although it may be possible to derive  $v \sin i$  even if its value is smaller than  $\zeta_{RT}$ , the detection and measurement of surface *differential* rotation of slowly rotating stars from spectral line profiles is an unsolved question at least in practice (e.g., Gray & Baliunas 1997). The detection and measurement of differential rotation from observation of non-radial stellar pulsations like the 5 min oscillations of the Sun is an outstanding task and requires an observational accuracy which has not yet been reached from terrestrial sites.

The only method which is practical at present is the observation of stellar butterfly diagrams: i.e., monitoring the rotation period over an activity cycle. The basic idea is that (by analogy with the Sun) active regions (ARs) appear in two belts on the stellar surface at mid-latitudes (one in each hemisphere) at the beginning of an activity cycle, and shift monotonically towards the equator as the cycle progresses.

Stellar butterfly diagrams have been observed using survey data from Mount Wilson Observatory’s HK Project (Baliunas et al. 1985; Donahue 1993). The presence of SDR has been detected for the Sun and 36 lower main-sequence stars with various spectral types, ages and rotation periods. As many as

six different patterns have been identified showing changes in rotation period with time, or where possible, phase of the activity cycle (Donahue 1993; Donahue & Baliunas 1994). In some cases, stars with nearly identical parameters (i.e., mass and age) show completely different butterfly diagrams. This raises some questions, in particular, whether artifacts in the data can produce errors or inaccuracies in the determination of rotation period. Donahue (1993) notes that an important influence upon the determination of rotation period is active region growth and decay (ARGD).

ARGD appearing simultaneously at different stellar longitudes, will produce variability of not only the observed amplitude, but also the phase of rotational modulation, possibly including variations of the period. In those cases a deviation from sinusoidal modulation is also expected. Further, SDR can produce a multi-periodic signal caused by ARs positioned at different latitudes; the well-known butterfly-diagram of the Sun (Maunder 1913; Yallop & Hohenkerk 1980) shows that spots appear at a variety of latitudes at any given time. Hence, measurements of the gross rotation period will be variable on time-scales which are shorter than the activity cycle. Despite the possibility of strong scatter of the measured rotation period at shorter time-scales, we can hope that a general trend will be visible provided the length of the time series observed is sufficient to see this trend and, if the number of observations per time interval is large enough to determine the parameters of rotational modulation with sufficient precision.

This expectation must first be tested with the Sun; it is the only star for which we know both the differential surface rotation and can trace the appearance and disappearance of specific AR's on the stellar surface in detail. Although the pattern of surface differential rotation derived from different observational tracers differs slightly, the solar surface differential rotation can be reasonably approximated by (cf., Lang 1992)

$$P_{\text{syn}} = 26.75 + 5.7 \cdot \sin^2 \phi, \quad (1)$$

where  $\phi$  is the solar latitude and  $P_{\text{syn}}$  is the synodic rotation period. Hence, assuming a possible AR latitude range  $40^\circ \geq \phi \geq 0^\circ$  a band-width  $29.1 \geq P_{\text{syn}} \geq 26.8$  d results. Donahue & Keil (1995) analysed a time series of disk-integrated Ca II K emission (Keil & Worden 1984) finding the correct qualitative behaviour: a jump from faster rotation to slower values at activity cycle minimum followed by a trend of increasing rotational velocity with cycle phase. Quantitatively, they derive a sidereal rotation period of 28.5 d at the beginning of Cycle 22, corresponding a synodic period of  $\approx 31$  days that is too large as Schrijver (1996) has recently criticized. It also seems that the decline of rotation period observed is too steep, reaching  $P_{\text{syn}} = 26.7$  d only five years later.

Because all of the parameters involved in detecting SDR are likely to also vary themselves (largely due to ARGD), a two-dimensional time-frequency analysis is preferred. In this paper we present the results of a wavelet analysis of disk-integrated solar Ca II K-line fluxes, including those analyzed by Donahue & Keil (1995).

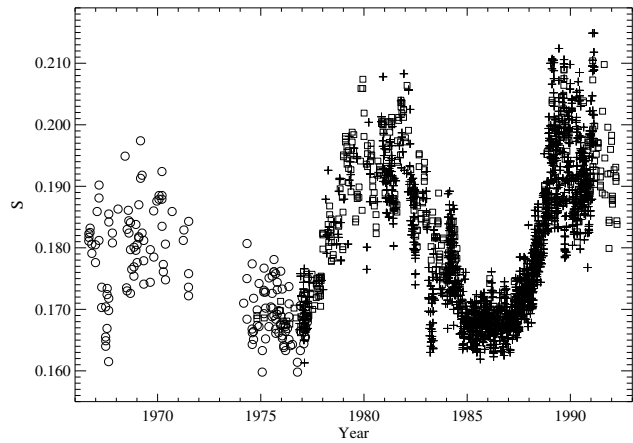


**Fig. 1.** The time series of solar disk-integrated Ca II K-line emission. Symbols are:  $\circ$  – Mount Wilson lunar measurements (Wilson 1978);  $\square$  – KPNO disk-integrated K-line flux (White & Livingston 1978, 1981);  $+$  – SPO disk-integrated K-line flux (Keil & Worden 1984; Keil 1992). The SPO and KPNO fluxes have been converted to the Mount Wilson  $S$  index (see text).

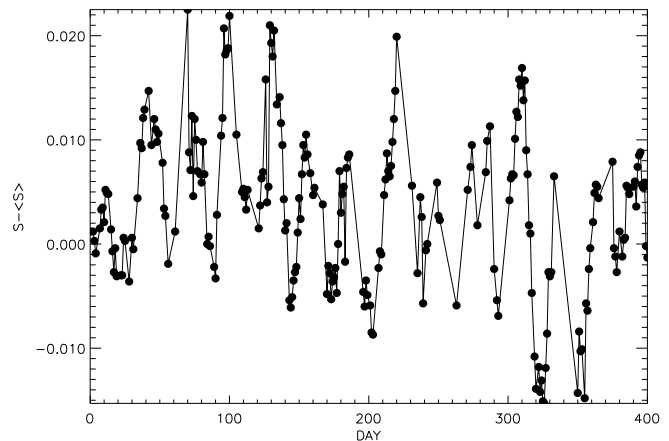


**Fig. 2.** A 400 d subsample during mid-1989 demonstrating strong variability of amplitude and phase of rotational modulation.

## 2. Observations

The data come from three sources: Wilson's (1978) observations of the Moon from 1966–1971 and 1974–1977 at Mount Wilson Observatory, plus two independent measurements of the disk-averaged K-line flux. Observations have been made at Kitt Peak National Observatory (KPNO) by White & Livingston (1978, 1981) since late 1974, and at Sacramento Peak Observatory (SPO) since 1976 (Keil & Worden 1984; Keil 1992). Donahue & Keil (1995) analyzed the solar SDR using the SPO data alone.

The SPO and KPNO K-line index has been converted to the Mount Wilson  $S$  index using the solar 10.7 cm flux as an intermediary (Baliunas et al. 1995). This is necessary because the K-line observations and Mount Wilson  $S$  observations do not overlap sufficiently to permit a direct calibration. The time

series is shown in Fig. 1. Nearly the entire time series is plotted by Baliunas et al. (1995) in their Fig. 1d.

In a first step the time-series was cleaned from long-term trends having its origin in the solar 11 y cycle. Fig. 2 shows a 400-day subsample of the cleaned data to demonstrate the rotational modulation. ARGD is clearly apparent in Fig. 2, and that all of the parameters related to rotational modulation are strongly variable on time-scales spanning only a few rotational cycles.

In a second step we have placed the data into daily bins and further, the observational gaps in the time series were filled with zeroes because our wavelet code is written for equally spaced data.

### 3. Data analysis

Several methods are generally used to study the time-dependence of a periodic signal. A very popular example from variable star research is the so-called ‘O–C diagram’ in which deviations between the observed and the predicted zero-phases of the signal are depicted over time. This method requires a sufficient signal-to-noise ratio, and good phase coverage because the signal must be ‘visible’. Another often-used method is to subdivide the time series, and analyzing each sub-sample separately through periodogram analysis (Scargle 1982; Horne & Baliunas 1986). Using this method, Baliunas et al. (1985) and Donahue (1993) examined the year-to-year variations of the rotation periods of several solar-like stars (stellar butterfly diagrams). A more sophisticated method is the collection of Fourier transforms of subsamples formed by a window propagating over the entire series. This constitutes the Gabor transform. However, one disadvantage of the Gabor transform is that the number of oscillations inside the window depends on the frequency analyzed. Thus, the relative frequency resolution will vary over the frequency interval studied.

The wavelet transform uses a window whose width is a function of the actual frequency. Several types of wavelets can be used. However, if the signal is sinusoidal, the wavelet should also be chosen to be sinusoidal. Thus, the Morlet wavelet (Grossmann & Morlet 1984)

$$W(t) = e^{-a(\nu(t-\tau))^2} e^{i2\pi\nu(t-\tau)} \quad (2)$$

represents a sinusoidal oscillation contained within a Gaussian envelope. Then the wavelet transform can be written as

$$WT(\nu, \tau) = \sqrt{2\pi\nu} \int S(t) W^*(\nu(t-\tau)) dt, \quad (3)$$

where  $W^*$  is the complex conjugate of  $W$ . The discrete wavelet transform is

$$WT = \sqrt{2\pi\nu} \sum_j S_j(t_{j+1} - t_j) e^{-a(\nu(t_j-\tau))^2} e^{-i2\pi\nu(t_j-\tau)} \quad (4)$$

where  $S_j = S(t_j)$ . The parameter  $a$  controls the resolution in both frequency and time (Baudin et al. 1994):

$$\Delta\tau = \frac{1}{\nu} \sqrt{\frac{\ln 2}{a}}, \quad \Delta\nu = \frac{\nu}{\pi} \sqrt{a \ln 2}. \quad (5)$$

Therefore, the relative frequency resolution is uniquely determined by  $a$ , whereas the time resolution depends on the frequency itself to hold the number of oscillations inside the wavelet constant. We choose  $a = 0.005$  in our analysis in order to balance the time and frequency resolution.

To evaluate the time-frequency behaviour we plot a wavelet map as the square of  $WT(\nu, \tau)$  (the ‘power’) with dependence on time and frequency as a first step. A visual inspection of such a plot shows regions of enhanced power which, in case of a positive detection of the SDR, will follow systematic trends in the form of one or more ‘mountain ranges’ or, even in a more complicated manner, as a series of isolated peaks as the peak frequency changes over the course of the activity cycle. Next, cuts are made along the frequency axis at discrete values of time, in order to find the absolute maximum power and also the relative maxima of power at each epoch and their corresponding frequencies. In the third step, these frequencies are plotted over time. This plot will represent a stellar butterfly diagram, i.e. the time evolution of rotation periods that are defined by the rotation experienced by plage regions causing modulation of the emission core of the solar disk-integrated Ca II K line.

As in the case of Fourier analysis of unevenly sampled data, artifacts may result which can lead to misinterpretation of the wavelet map. Szatmáry, Vinkó & Gál (1994: SVG94) investigated the properties of the wavelet map in the cases of the following signal characteristics: i) varying amplitude, period, and zero-phase; ii) strong deviations of the signal from a sine curve; iii) double-mode oscillations; iv) the influence of noise; and, v) gaps in the time series. Based on their analysis, we assume the following expected characteristics might be found in wavelet pictures of our time series:

i) Fig. 2 shows that strong variations in amplitude, period, and phase exist, even on timescales close to the rotation period. A variable amplitude will lead to a variation of power with time, whereas jumps in zero-phase can disrupt a ‘mountain range’ into isolated peaks. A further loss of power occurs because the original data are unevenly sampled, and while filling in the time series with zeroes causes it to *appear* evenly spaced, the additional points complicate the wavelet map by re-distributing power randomly. A similar effect results from the existence of seasonal gaps in the data that are typical for stellar observations, although not present in the solar time series considered here. While the systematic changing of the period by SDR should be visible in the wavelet map the Fourier analysis of the time series as a whole will lead to a broadening of the Fourier peak only, making it impossible to derive period shifts and jumps within the time series. The ability to investigate the time-dependence of the oscillating parameters is an important advantage of wavelet analysis. Furthermore, jumps of the phase caused by the eruption of multiple ARs at different stellar longitudes should be visible in the wavelet map, while this same behaviour causes frequency splitting in the discrete Fourier transform (Donahue 1993). However, SVG94 uses a sufficiently short window in order to resolve the temporal behaviour in detail. In our case, the time-resolution will be chosen to be low enough to hold the frequency resolution required. In

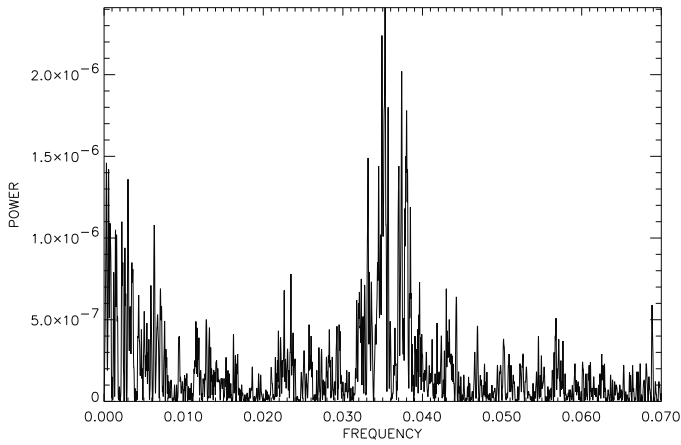


**Fig. 3.** Fourier power spectrum of the solar data from 1967 until 1992

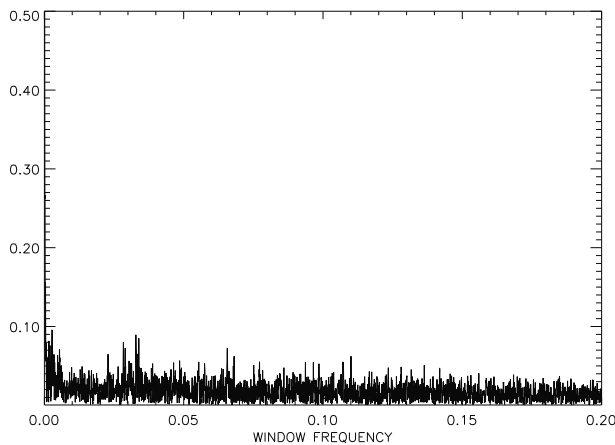


**Fig. 4.** The window function.

fact, in selecting  $a = 0.005$  the corresponding time resolution ( $\sim 300$  d) will likely smooth much of the variability at shorter time-scales as might be caused by ARGD. Hence, the evolution of ARs might remain invisible. One can expect, therefore, that zero-phase modulation as caused by ARGD at different stellar longitudes will produce some artifact in the form of side-lobes in the wavelet map. The reason is quite simple: as the time-resolution decreases, the differences between Fourier analysis and wavelet analysis also decrease. Fig. 12 of SVG94 shows that zero-phase modulation will produce a complex pattern of peaks in the wavelet map at high time-resolution whereas the Fourier spectrum shows side-lobes. We can therefore assume that the corresponding wavelet map of low time-resolution will also show side-lobes in form of mountain ranges beside the dominant mountain range.

ii) Deviations from a sine curve will have little influence because strong deviations such as those in the light curve of eclipsing binaries cannot be expected.

iii) Double-mode oscillations can arise from two ARs at different latitudes. The behaviour of the wavelet spectrum will depend on the time resolution because the superposition of two

signals leads to a complicated but regular pattern in the time series. If the time-resolution is fine enough, the pattern will be visible in the wavelet map; otherwise the wavelet picture is no more informative than the Fourier spectrum, i.e., there will be two parallel mountain ranges in the wavelet map. If the two modes are close together in frequency; a beat phenomenon is expected. In this case, the wavelet map looks like amplitude modulation. Mode switching can, in principle, be localized in time which cannot be examined using Fourier analysis.

iv) The influence of low amplitude noise on wavelet analysis is similar to its effect on Fourier analysis. However, in the case of strong noise, the Fourier spectrum is a better tool simply because the maximum number of data points is included in a window that has the maximum length possible.

v) Gaps in the data are quite usual for stellar observations. Under certain circumstances they can produce side-lobes in the wavelet map, similar to ‘aliases’ seen in Fourier analysis (Horne & Baliunas 1986). In this particular investigation, large (seasonal) gaps are not present; the characteristic gap size in this time series is only on the order of a few days.

## 4. Results

### 4.1. Fourier analysis

The first question as to whether the rotation period is visible at all can be answered by Fourier analysis of the time series as a whole, i.e., the solution without time-resolution. In Fig. 3 we show the power spectrum resulting from application of Breger’s PERIOD code (Breger 1990) applied to the entire time series. Apart from the appearance of enhanced power at low-frequencies ( $\lesssim 0.01$  cycles/day) which arises from a non-perfect fit of the solar cycle, the spectrum is clearly dominated by the solar synodic rotation: maximum power appears at a period of 28.3 days. This would correspond to the solar rotation at latitude  $30^\circ$  where active regions are concentrated at the beginning of the solar cycle. A second (but less dominant) peak appears at a period of 26.8 days corresponding to the solar rotation rate at latitude  $5^\circ$ , the latitude of the active zone near the end of the solar cycle. Surprisingly, there is also a third peak at a period of 30.2 days which would require the existence of ARs at a latitude of  $50^\circ$ . This peak is likely an artifact resulting either from the window function or from ARGD (cf., Sect. 3). The window function (Fig. 4) does not show any enhanced frequencies. Hence, the 30.2 d period cannot be the result of the data sampling: a time-resolved analysis is required to uncover its nature.

Another surprising feature to Fig. 3 is that the 28.3 d and the 26.8 d periods are clearly separated from each other. If there were a continuous shift of AR’s in latitude during a solar cycle one would expect a single but very broad peak to appear in the power spectrum. The existence of two separate peaks could possibly be explained by the uneven distribution of power at isolated times, for example, at the beginning and the end of a solar cycle. Power might be reduced at solar maximum because the number of ARs at different longitudes is large enough that rotational modulation is smeared out and power is reduced.

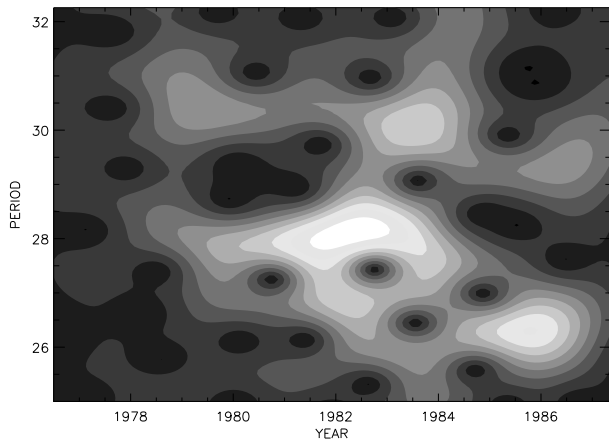


**Fig. 5.** Wavelet map of cycle 21 from 1977 until 1987 shown as a contour plot above the time-period plane.

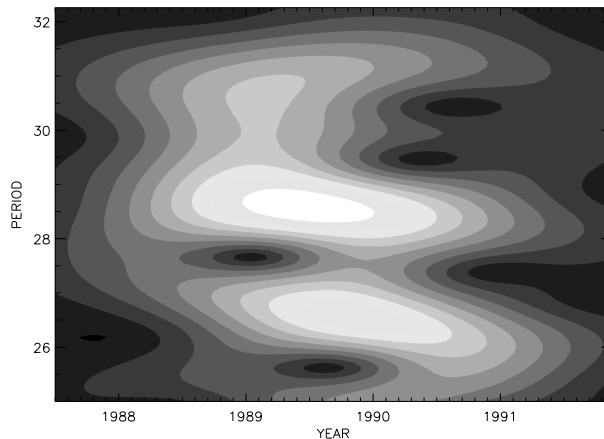


**Fig. 6.** Wavelet map of cycle 22 from 1987 until 1992.

#### 4.2. Wavelet analysis

In a first step we have applied the wavelet transform to the whole time series including cycles 20–22. However, the data sampling before 1977 is poor compared to the years afterwards. The wavelet map, a three-dimensional plot of power as a function of time and frequency, looks quite different for these two intervals. The wavelet map after 1977 is rich with ranges of peaks, while the map from the early years (cycle 20) is almost empty. Therefore, we have concentrated our subsequent analysis to Cycles 21 and 22, only.

The wavelet plot of Cycle 21 (Fig. 5) shows a broad mountain range with a tendency to fall from  $\approx 28$  d (in 1978) to  $\approx 26$  d near the end of that cycle. This range is structured as individual peaks, but there is a second (but much weaker) mountain range adjacent to the main range at longer ( $\gtrsim 30$  d) periods. This could be the wavelet answer to the appearance of the 30.2 d period found from Fourier analysis above. The time-resolution of  $\approx 1$  y and the period resolution of  $\approx 0.5$  d do not allow for a more-detailed examination. However, from slices made at a series of epochs it is clear that there are several maxima of power present at any given time even within the prominent mountain range (e.g., during 1983).

The wavelet plot of Cycle 22 (Fig. 6) is characterized by two rather straight mountain ranges where the more prominent range follows the same values as the primary mountain range of Cycle 21. As in case of Cycle 21, there is a spurious third range near 30 days. Somewhat surprising is the comparatively strong power of the second range. Obviously it has its analogy in the strong 26 d side-lobe in the Fourier spectrum (Fig. 3). It cannot be due to rotation alone because the period falls below the limit given by Eq. (1). We discuss its possible nature below.

We assume that the prominent mountain ranges of both Figs. 5 and 6 reflect the true rotation period from three reasons: first, from the fact that maximum power is concentrated there in both Cycle 21 and Cycle 22; and second, that the 26 d range is only visible during Cycle 22 whereas it is absent during Cycle 21. Finally, the values of  $P_{\text{syn}}$  inside the dominant range

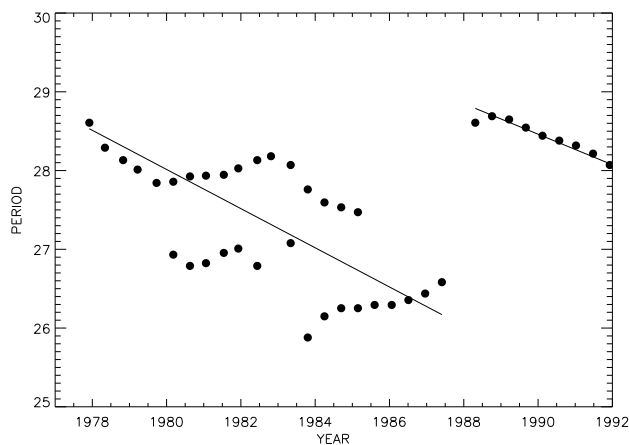


**Fig. 7.** ‘Stellar butterfly diagram’ of the Sun.

are reasonable, lying within the interval given by Eq. (1) such that  $0^\circ \leq \phi \leq 40^\circ$ .

To record changes in rotation period we have made cuts along the period axis at specific intervals of time with a time resolution typically half of the intrinsic wavelet resolution of  $\approx 1$  y. In Fig. 7 the periods of all maxima found along those cuts but inside the prominent mountain range are plotted versus time (dots). Then weighted least squares fits were made where the weights were set proportional to the power of a given maximum (the two straight lines in Fig. 7).

Fig. 7 shows a ‘stellar butterfly diagram’ close to what is expected for the Sun: the fits yield a synodic period of 28.6 d at the early phase of Cycle 21, and 26.5 d at the end of this cycle. However, the latter value is a bit too low, lying below the 26.75 d limit at the solar equator. Then, the new cycle starts again with a 28.6 d period and decreases with nearly the same slope as Cycle 21. If one extrapolates the line towards 1998 (the expected year of the end of this cycle), then a synodic period of 26.9 d is found, which is a reasonable value at solar activity minimum.

## 5. Discussion and conclusion

Our time series analysis of solar disk-integrated Ca II K emission using the wavelet transform yields nearly the correct pattern of SDR. Maximum values of periods are found at the beginnings of Cycle 21 and Cycle 22. Over the course of both cycles, the period decreases systematically with almost the same rate of decline. There is also a clear transition from low to high values of rotation period between the end of Cycle 21 and the start of Cycle 22. Thus, the qualitatively correct behaviour is found. However, the quantitative behaviour is more complex. Several peaks are seen simultaneously and the slope of increasing rotation rate over the activity is not smooth, at least for Cycle 21.

It is known from monitoring of the sunspot cycle that spots appear at a variety of latitudes at any given time, and that the latitude spread in the solar butterfly diagram is large. Therefore, the large scatter in the 'stellar' butterfly diagram seen here should be expected. However, the scatter will be reduced by smoothing resulting both from the low time and frequency resolutions. A time-resolution of one year will smooth any internal pattern resulting from ARGD. Insofar our wavelet map will reflect an averaged behaviour, this is really what is of interest.

Compared with the observed disk-resolved differential rotation of the Sun, our result is reasonable. According to Eq. (1), and taking into account that at early phases of a solar cycle spots appear around  $30^\circ$  one expects a rotation period of  $\approx 28.5$  d, and at the end of a cycle approximately 27 d. Indeed, we find the correct value at the beginnings of both cycles. However, there is a slight deviation of  $-0.5$  d at the end of Cycle 21 in 1987. This deviation is small because one has to take into account the low frequency resolution which corresponds to a uncertainty of 0.5 d.

Cycle 22 shows two large mountain ranges with somewhat peculiar behaviour. While the range with the longer period dominates, the second range is also powerful and therefore cannot be neglected. The question is whether this period splitting is of intrinsic nature or if it is an artifact of some kind? Szatmáry et al. (1994, c.f. Sect. 3) list three possibilities: double mode oscillation, phase modulation on a time-scale smaller than our chosen time resolution or regular gaps in the data. Since there are no regular gaps, the remaining possibilities are double mode oscillation or phase modulation.

Double mode oscillation could result from the preferred appearance of plage regions at high and low latitudes, but with a lack of those regions at intermediate latitudes – possibly arising from an asymmetry between the northern and the southern hemispheres. Phase modulation must also be expected because of the appearance of active regions at different solar longitudes, which in connection with ARGD, will not only modulate the zero phase, but will also shorten or lengthen the period of rotational modulation. This is indeed the case demonstrated in Fig. 2. Because our time-resolution is much too small to follow the ARGD of the individual ARs, side-lobes can appear in the wavelet map as discussed in Sect. 3. This could also be the reason for the third but very weak mountain range found in the

wavelet picture around  $\approx 30$  d. This range cannot be explained by appearance of plages at high latitudes because it would involve the existence of plages latitude  $50^\circ$  and higher – not seen in the disk-resolved data.

We can conclude from the subsequent observation of stellar butterfly diagrams it should be possible to derive the sign and magnitude of the period change over the activity cycle. Therefore, wavelet analysis appears to be an effective tool to investigate stellar differential rotation by observation of stellar butterfly diagrams. However, the appearance of side-lobes in the wavelet picture must be handled with some caution and could possibly be caused by active region growth and decay rather than by two independent active belts or by a north-south asymmetry in activity.

*Acknowledgements.* We thank S. Keil of the U.S. National Solar Observatory (SPO) for making his data available to us, and to W.C. Livingston and O.R. White for the KPNO solar data, and to Tim Henry for his diligence and care in reducing the solar spectra. A.H. wishes to thank Tilo Jankowsky and Manfred Schultz (AIP) for his care in computer programming.

## References

- Baliunas S.L., et al., 1985, *ApJ* 294, 310
- Baliunas S.L., et al., 1995, *ApJ* 438, 269
- Baudin F., Gabriel A., Gilbert D., 1994, *A&A* 285, L29
- Breger M., 1990, *Communications in Asteroseismology*, No. 20
- Donahue R.A., 1993, Thesis PhD, New Mexico State University
- Donahue R.A., Baliunas S.L., 1994, in: *Cool Stars, Stellar Systems and the Sun*, ed. J.-P. Caillault, ASP Conf. Ser. 64, 396
- Donahue R.A., Keil S.L., 1995, *Solar Phys.* 159, 52
- Gray D.F., 1988, in: *Lectures on spectral line analysis: F,G and K stars*, University of Western Ontario, p. 3.8
- Gray D.F., Baliunas S.L., 1997, *ApJ* 475, 303
- Grossman A., Morlet J., 1984, *SIAM J. Math. Anal.* 15, 723
- Horne J.H., Baliunas S.L., 1986, *ApJ* 302, 757
- Keil S.L., 1992, private communication to R.A. Donahue
- Keil S.L., Worden S.P., 1984, *ApJ* 276, 766
- Kennedy J.R., 1996, *Sky & Telescope* 92, 20
- Kitchatinov L.L., Rüdiger G., 1995, *A&A* 299, 446
- Küker M., Rüdiger G., Kitchatinov L.L., 1993, *A&A* 279, L1
- Lang K.R., 1992, 'Astrophysical Data: Planets and Stars', Springer-Verlag New York etc., p. 104
- Libbrecht K.G., 1988, in: *Seismology of the Sun and Sun-like Stars*, ed. J. Rolfe, ESA Sp-286, 131
- Maunder E.W., 1913, *MNRAS* 74, 112
- Rüdiger G., Kitchatinov L.L., 1994, in: *The solar engine and its influence on terrestrial atmosphere and climate*, ed. E. Nesme-Ribes, NATO ASI Series, Vol. 25, Springer-Verlag Berlin, p. 27
- Scargle J.D., 1982, *ApJ* 263, 875
- Schrijver C.J., 1996, in: *Stellar surface structure*, eds. K.G. Strassmeier and J.L. Linsky, Kluwer Academic Publishers, p. 1
- Szatmáry K., Vinkó J., Gál J., 1994, *A&ASS* 108, 377
- Wilson O.C., 1978, *ApJ* 226, 379
- White O.R., Livingston W.C., 1978, *ApJ* 226, 679
- White O.R., Livingston W.C., 1981, *ApJ* 249, 798
- Yallop B.D., Hohenkerk C.Y., 1980, *Sol. Phys.* 68, 303